Integrated optical- and acoustic-resolution photoacoustic microscopy based on an optical fiber bundle

Wenxin Xing,[1,2,†] Lidai Wang,[1,†] Konstantin Maslov,[1] and Lihong V. Wang[1,2,*]

[1]*Optical Imaging Laboratory, Department of Biomedical Engineering, Washington University in St. Louis, One Brookings Drive, St. Louis, Missouri 63130, USA*

[2]*Preston M. Green Department of Electrical and Systems Engineering, Washington University in St. Louis, One Brookings Drive, St. Louis, Missouri 63130, USA*

**Corresponding author: lhwang@wustl.edu*

Received August 30, 2012; revised November 15, 2012; accepted November 27, 2012; posted December 4, 2012 (Doc. ID 175121); published December 20, 2012

Photoacoustic microscopy (PAM), whose spatial resolution and maximum imaging depth are both scalable, has made great progress in recent years. However, each PAM system currently achieves only one resolution with an associated maximum imaging depth. Here, we present an integrated optical-resolution (OR) and acoustic-resolution (AR) PAM system implemented by delivering light via an optical fiber bundle. A single fiber core is used to deliver light for OR illumination in order to achieve a small spot size and hence high lateral resolution, whereas all the fiber cores are used to deliver more energy for AR illumination. Most other components are shared by the OR and AR imaging. The lateral resolution can be seamlessly switched between 2.2 and 40 μm as the maximum imaging depth is switched between 1.3 and 3.0 mm. The system enables automatically coregistered higher-resolution OR and deeper AR photoacoustic imaging. © 2012 Optical Society of America

OCIS codes: 170.3880, 170.5120.

Due to its optical absorption contrast and high spatial resolution that is scalable with the maximum imaging depth, photoacoustic microscopy (PAM) has been successfully applied to *in vivo* imaging at scales from organelles to organs [1,2]. According to their different lateral resolutions, PAM systems can be categorized into either acoustic-resolution (AR) PAM or optical-resolution (OR) PAM. AR-PAM [3,4], whose lateral resolution is determined by the acoustic focus, can achieve tens of micrometers lateral resolution with a maximum imaging depth of several millimeters. OR-PAM [5,6] has a tighter optical focus than acoustic focus and can achieve optical-diffraction-limited lateral resolution with a maximum imaging depth of ~1.2 mm [7]. With these complementary characteristics, AR- and OR-PAM systems have been used in tandem to image samples in many applications [8,9]. However, since the systems share similar optical and ultrasonic components and designs, it is advantageous to combine them, which would facilitate either sequential or simultaneous operation, yielding automatically coregistered images and also reducing system cost. Here, we present a method to integrate OR- and AR-PAM systems based on an optical fiber bundle.

A schematic of the system setup is shown in Fig. 1. A high-repetition-rate laser (SPOT 10-200-532, Elforlight) provides photoacoustic excitation for OR imaging, whereas a high-power laser (Cobra, Sirah) pumped by a Nd:YLF laser provides photoacoustic excitation for AR imaging. The high-repetition-rate laser operates at 532 nm, near the 530 nm isosbestic absorption wavelength of oxy- and deoxy-hemoglobin. The high-power laser is tuned to another isosbestic point at 570 nm, where optical absorption of hemoglobin is comparable with that at 532 nm. Emerging from the lasers, both beams are vertically polarized. The AR beam becomes horizontally polarized upon reflection off two mirrors M1 and M2. In contrast, the OR beam is focused by a condenser lens (LA1214-A, Thorlabs), then spatially filtered by a 25 μm diameter pinhole positioned slightly after the focus. The two laser beams are combined by a polarizing beam splitter cube (PBS201, Thorlabs). Because of the cube's high extinction ratio, most of the beam energy propagates toward the fiber coupler (F-91-C1, Newport, with a 10 × magnification objective lens). A fiber bundle (IGN-037/10, Sumitomo) is used to achieve switchable OR and AR illumination. A single core (diameter: 2.0 μm) is used to deliver OR light in order to achieve a small spot size and hence high lateral resolution, whereas all the 10,000 fiber cores are used to deliver more energy for AR illumination. To focus the OR beam onto a single core of the fiber bundle, the tip of the fiber bundle is aligned at the focus of the OR beam. In the meantime, the AR beam is defocused at the tip, and its beam size is properly expanded (1.5 × magnification) by a beam expander (not shown in Fig. 1) placed between mirrors M1 and M2, so that the beam spot can fill all

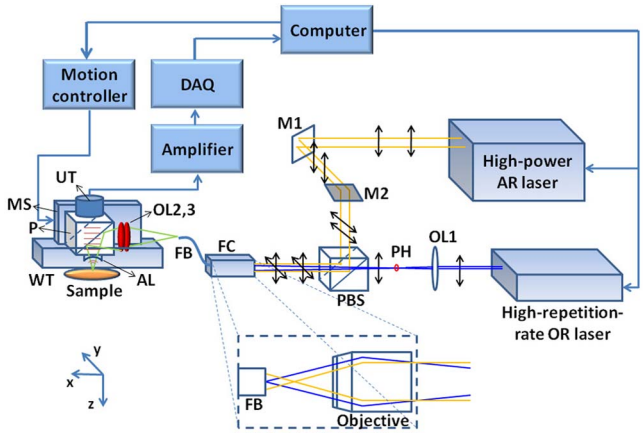

Fig. 1. (Color online) Schematic of the integrated AR and OR PAM system. The interior of the fiber coupler is zoomed in the dashed box. AL, acoustic lens; DAQ, data acquisition card; FB, fiber bundle; FC, fiber coupler; M1 and M2, mirrors; MS, motor stage; OL1, OL2, and OL3, optical lens; P, prism; PBS, polarizing beam splitter; PH, pinhole; UT, ultrasound transducer; WT, water tank.

 © 2012 Optical Society of America

the cores of the bundle at the tip (shown in the dashed box in Fig. 1).

The other end of the fiber bundle is mounted to a photoacoustic scanning stage. The laser beams emerging from the fiber bundle pass through two identical optical condenser lenses, reflect off the aluminum-coated hypotenuse of a prism, and then focused into the sample. The generated photoacoustic signal is collected by the acoustic lens, which is in confocal arrangement with focused laser beam, and then received by a 50 MHz ultrasound transducer (V214, Olympus NDT). The electrical signal from the ultrasonic transducer is amplified, digitized, and analyzed by a personal computer, which also synchronizes the motion controller with the DAQ card and the lasers. A more detailed description on fast voice-coil scanning can be found in our previous publication [10]. Since the photoacoustic probe weighs less than 40 g as our previous one, the fast scanning ability is maintained in the integrated OR/AR-PAM system.

To evaluate the performance of the system, the spatial resolutions and maximum imaging depths for both OR and AR imaging were measured in a series of experiments. All experimental animal procedures were carried out in conformity with the laboratory protocol approved by the Animal Studies Committee at Washington University in Saint Louis. The fluence at the surface is constantly maintained below the American National Standards Institute (ANSI) safety limit, 20 mJ $/cm^2$ at the chosen wavelengths [11]. A resolution target (1951 USAF Hi-Resolution Targets, Edmund Optics) was imaged in water with only OR-PAM. The entire image of groups 6–9 is shown in Fig. 2(a), and a partial close-up is shown in Fig. 2(b). The system can resolve element 6 in group 8 [arrow in Fig. 2(b)], with 456 line pairs per millimeter, which translates into an OR imaging lateral resolution finer than 2.2 μm. The discrepancy from the theoretical resolution of 1.4 μm (NA: 0.2, wavelength: 532 nm) may be attributed to optical aberration and higher-order modes of the optical fiber. The lateral resolution of the AR imaging was evaluated by imaging a 6 μm diameter carbon fiber as an approximate line target. The lateral full width at half-maximum (FWHM) is 40 μm, as shown in Fig. 2(c). Since the axial resolution is determined by the acoustic parameters only, the OR and AR imaging share the same axial resolution. We used two methods to evaluate the axial resolution. As shown in Fig. 2(d), the enveloped axial line spread function (LSF) has a FWHM of 29.3 μm, which shows how wide the image of a single line source appears. The resolution based on the shift-and-sum method [12]—which mimics the combined image as two line sources approach each other—is ~16 μm at a contrast-to-noise ratio (CNR) of 2.0, as shown in Fig. 2(e). Figures 2(f) and 2(g) show the OR and AR images of a black needle that was obliquely inserted in the leg of an anesthetized mouse, where time-gain compensation was applied to enhance deeper signals. For OR-PAM, the needle is visible at depths down to 1.2 mm, and blood vessels (arrows in the figure) can be imaged at depths down to 1.3 mm. The signal-to-noise ratio (SNR) of the blood vessel at 1.3 mm is 2.6. For AR-PAM, the maximum imaging depth is 3.0 mm with an SNR of 2.0.

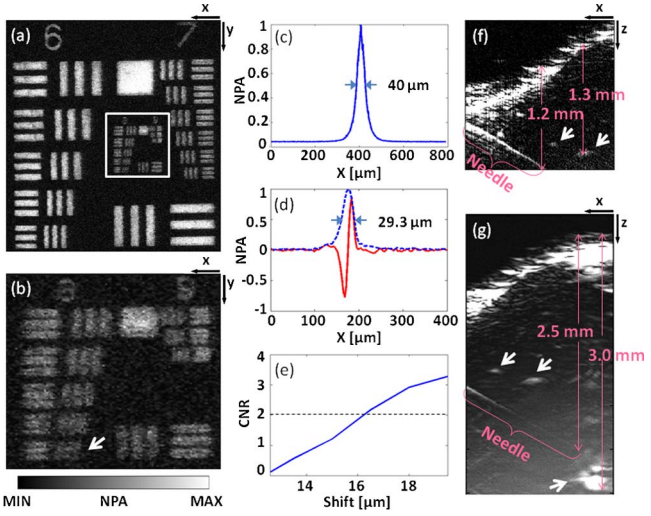

Fig. 2. (Color online) System performance test of the integrated OR/AR-PAM system. (a) OR-PAM image of a resolution test target and (b) its close-up. (c) Lateral LSF of the AR-PAM. (d) Axial LSF (red solid curve) and its envelope (blue dashed curve). (e) CNR versus shift. (f) *In vivo* OR- and (g) AR-PAM images of a black needle and blood vessels (marked by arrows) in a mouse leg. CNR, contrast-to-noise ratio; NPA, normalized photoacoustic amplitude.

The integrated system can operate in two modes: switching and simultaneous modes. In switching mode, as in regular microscopy with switchable objectives, OR- and AR-PAM operates sequentially. The ear of a nude mouse (Athymic Nude Mice, Harlan) was imaged *in vivo* to demonstrate this mode. The mouse was anesthetized by isoflurane and positioned on an animal platform. A large area of the ear was first imaged by AR-PAM, as shown in the maximum amplitude projection image in Fig. 3(a), which reflects the distribution of total hemoglobin concentration in relative values. Then a small region of interest was imaged by OR-PAM [Fig. 3(b)]. Due to the high resolution, the imaged region appears with more details, including single microvessels and red blood cells (RBCs).

In simultaneous mode, the two lasers are triggered alternately, each firing at its own pulse repetition rate.

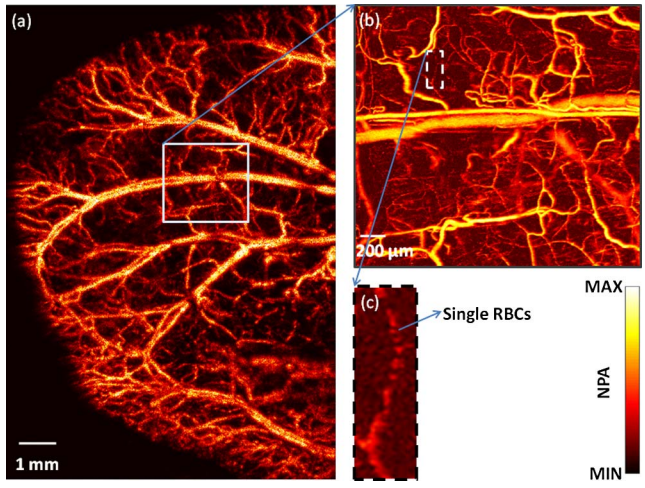

Fig. 3. (Color online) Image of a mouse ear. (a) Large region of the mouse ear imaged by AR-PAM. (b) Region of interest imaged by OR-PAM. (c) Close-up image showing single RBCs.

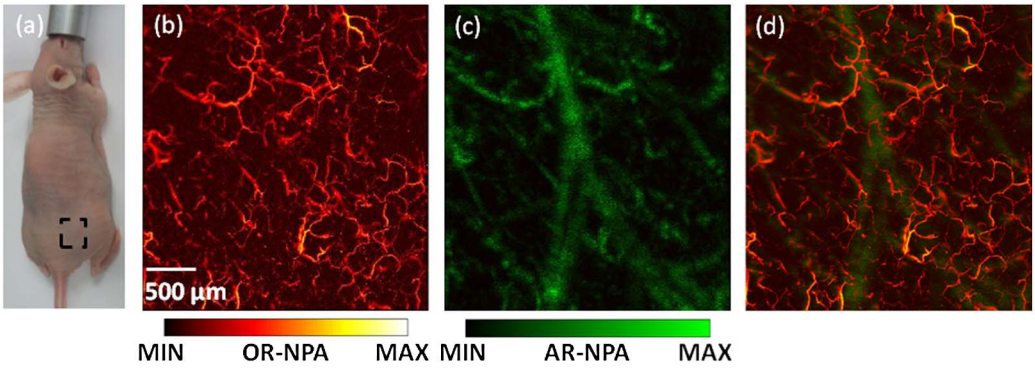

Fig. 4. (Color online) Combined PAM images of mouse back. (a) Photograph of the mouse. The region of interest is highlighted in the dashed box. (b) OR-PAM image of skin. (c) AR-PAM image. (d) Overlaid PAM image (see Media 1). OR-NPA, normalized photoacoustic amplitude in OR image; AR-NPA, normalized photoacoustic amplitude in AR image.

The OR laser fires with less energy than the AR laser. For highest resolution, the OR laser is triggered with every step of the motor scanning, while the AR laser is triggered only once in 10 steps. Every 10th step, OR-PAM and AR-PAM fire successively with a small intervening time interval; hence, the signals do not interfere with each other. The optical focus is aligned above the exact acoustic focus, but still within the acoustic depth of field. Thus, the integrated PAM system can simultaneously generate an OR image focused at one depth and an AR image focused deeper, which matches the anatomy that blood vessels in a superficial layer of skin are relatively small while large vessels are deeper [13]. Because the optical focus is kept in the acoustic depth of field, the sensitivity for OR-PAM detection was only slightly affected (less than 3 dB loss). As shown in Fig. 4(a), a region on the back of a nude mouse (Athymic Nude Mice, Harlan) was imaged *in vivo* in this mode. The OR and AR images [Figs. 4(b) and 4(c)] were acquired simultaneously in one single scan, with step sizes of 2 and 20 μm and laser repetition rates of 20 and 2 kHz, respectively. The AR image shows fewer small, shallow blood vessels than the OR image, but clearly shows the large, deep vessels that the OR image does not show. The merged image [Fig. 4(d) and Media 1] shows both small, shallow vessels acquired by OR-PAM and large, deep vessels acquired by AR-PAM.

In summary, the integrated system has successfully achieved switchable spatial resolutions and maximum imaging depths using an optical fiber bundle. To our knowledge, this is the first system that can perform OR and AR photoacoustic imaging simultaneously. The method we present here requires only modest modifications to current widely used PAM systems. Not limited to the two illumination choices introduced in this Letter, the fiber bundle allows a wide range of illumination spot sizes, from one single core to the entire core area, and optical scanning among the cores is also possible [14]. A double clad [15] or multiple clad fiber may be applied to provide flexible illumination spot sizes as well. This new integrated OR/AR-PAM system can bring multiscale imaging capability to many applications, such as anatomic imaging and label-free measurement of oxygen saturation.

This work was sponsored by National Institutes of Health (NIH) grants R43 HL106855, R01 EB000712, R01 EB008085, R01 CA134539, U54 CA136398, R01 CA157277, and R01 CA159959, as well as the Cancer Frontier Fund. L. V. Wang has a financial interest in Microphotoacoustics, Inc., and Endra, Inc., which did not support this work. K. Maslov has a financial interest in Microphotoacoustics, Inc., which did not support this work. The authors appreciate Prof. James Ballard's close reading of the manuscript.

†Authors contributed equally to this work.

References

1. L. V. Wang and S. Hu, Science **335**, 1458 (2012).
2. P. Beard, Interface Focus **1**, 602 (2011).
3. H. F. Zhang, K. Maslov, G. Stoica, and L. V. Wang, Nat. Biotechnol. **24**, 848 (2006).
4. L. D. Liao, C. T. Lin, Y. Y. I. Shih, T. Q. Duong, H. Y. Lai, P. H. Wang, R. Wu, S. Tsang, J. Y. Chang, and M. L. Li, J. Cereb. Blood Flow Metab. **32**, 938 (2012).
5. K. Maslov, H. F. Zhang, S. Hu, and L. V. Wang, Opt. Lett. **33**, 929 (2008).
6. Z. Xie, S. Jiao, H. F. Zhang, and C. A. Puliafito, Opt. Lett. **34**, 1771 (2009).
7. S. Hu, K. Maslov, and L. V. Wang, Opt. Lett. **36**, 1134 (2011).
8. C. P. Favazza, S. Hu, V. Huang, O. Jassim, L. A. Cornelius, and L. V. Wang, Proc. SPIE **7899**, 789946 (2011).
9. X. Cai, B. S. Paratala, S. Hu, B. Sitharaman, and L. V. Wang, Tissue Eng. Part C Methods **18**, 310 (2011).
10. L. Wang, K. Maslov, J. Yao, B. Rao, and L. V. Wang, Opt. Lett. **36**, 139 (2011).
11. Laser Institute of America, American National Standard for Safe Use of Lasers ANSI Z136.1-2007 (American National Standards Institute, 2007).
12. G. Ku, K. Maslov, L. Li, and L. V. Wang, J. Biomed. Opt. **15**, 021302 (2010).
13. I. M. Braverman, J. Investig. Dermatol. Symp. Proc. **5**, 3–9 (2000).
14. P. Hajireza, W. Shi, and R. J. Zemp, Opt. Lett. **36**, 4107 (2011).
15. S. Y. Ryu, H. Y. Choi, J. Na, E. S. Choi, and B. H. Lee, Opt. Lett. **33**, 2347 (2008).